Evaluating Data Transmission Performance in 5G mmWave Networks using Multi-Layer Transmission and MIMO Technology

John Baghous[1], and Mohamed Khaled Chahine[2]

***Abstract*—The transition from 4G to 5G networks was necessitated by fundamental limitations in spectral efficiency and data capacity inherent to the existing framework. Fifth-generation (5G) systems address these constraints by capitalizing on key enabling technologies, such as mmWave spectrum, multiple-input multiple- output (MIMO), massive MIMO (mMIMO), beamforming (BF) or Precoding. This paper investigates a multi-layer transmission scheme employing MIMO with Precoding (SVD) as a cooperative technique to enhance downlink (DL) data transmission performance in an enhanced mobile broadband (eMBB) scenario. The study operates within the standard 5G mmWave frequency band (FR2 at 40 GHz). We differentiate between key performance metrics: the user-experienced data rate (or throughput) Measured at the Receiver (Rx) and the peak theoretical data rate (or Bit Rate) Measured at the Transmitter (Tx). Simulation results, conducted using MATLAB, demonstrate that the proposed approach significantly improves both the achievable throughput and spectral efficiency within a fixed bandwidth. Throughput is evaluated in absolute terms (Mbps) and as a normalized percentage of the peak theoretical data rate (Bit Rate). The core of this study examines the impact of the number of spatial data streamng layers on a 5G-NR system performance. While increasing the transmission layers enhances the potential peak data rate at the transmitter, it concurrently elevates the bit error rate (BER) at the receiver, ultimately degrading the net throughput. This underscores the necessity for advanced receiver-side technologies, such as MIMO processing, to counteract high-path loss and other impairments prevalent at mmWave frequencies. The results confirm that augmenting the number of antennas in the MIMO configuration effectively mitigates this limitation. It improves the overall throughput and reduces the received BER by enhancing spatial diversity and signal recovery capabilities.**

***Index Terms*—mmWave, 5G, MIMO, massive MIMO, eMBB, multi-layer transmission scheme, CDL channel model, Data transmission, Bit Rate, Throughput, Spectrum efficiency.**

I. INTRODUCTION

5G technology, the fifth generation of wireless communication systems, represents a significant enhancement to global communication infrastructure, offering substantially higher data rates, lower latency, and greater network capacity [1,2].

[1] Department of Electronics and Communications Engineering, Faculty of Mechanical and Electrical Engineering, DU, Syria (DU e-mail: john.baghous@damascusuniversity.edu.sy) (Private e-mail: m.e.john.baghous@gmail.com)

[2] Department of Electronics and Communications Engineering, Faculty of Mechanical and Electrical Engineering, DU, Syria (e-mail: mk.chahine@damascusuniversity.edu.sy)

DOI: 10.36244/ICJ.2026.1.9

These systems enable a wide range of new applications across diverse fields such as manufacturing, healthcare, and intelligent transportation. This expansion, driven by the proliferation of data-intensive applications, has led to an exponential increase in user-generated data. Consequently, both academia and industry face the ongoing challenge of developing advanced techniques and technologies to meet rising demands and enhance the quality of service (QoS) for end-users [3].

As the number of connected devices continues to rise, global mobile data traffic is projected to grow by several orders of magnitude, with some estimates suggesting an increase of up to 20,000 times current volumes by 2030 [4]. This trend is already observable, with many countries reporting substantial annual growth in total data traffic [5].

This study investigates the prospective use cases for data transmission within the 37-40 GHz frequency band (n260 band as 3GPP TS 38.101-2), a spectrum specified in the 5G NR FR2 standard by 3GPP Release 15 and beyond. The simulation platform was fully developed and validated in compliance with the relevant 3GPP specifications to ensure standardization fidelity.

The remainder of this paper is organized as follows: Section II presents the adopted methodology and a concise overview of the key theoretical foundations. Section III details the practical system implementation and defines the performance metrics. Section IV presents and analyzes the simulation results. Finally, Section V provides a comprehensive discussion and concludes the paper.

II. Methods and Experiments

Given the infeasibility of conducting physical experiments and measurements, this study employed mathematical modeling, programming, and simulation as its primary methodological tools. This computational approach was deemed appropriate and sufficient for the defined research objectives.

The validity and accuracy of the implemented simulation platform were rigorously verified through a multi-faceted comparison. This included aligning the simulation outputs

with established mathematical models, benchmarking against performance tables and specifications outlined in relevant 3GPP technical reports and standards, and evaluating the consistency of curve behaviors and numerical trends with findings from prior research. All simulations were executed on a standard computing workstation using industry-standard software.

III. 5G System and Millimeter Wave Technology

South Korea pioneered the commercial deployment of 5G networks in March 2019. Since that initial launch, 5G technology has undergone substantial evolution and enhancement. The 5G system architecture is fundamentally designed to support three primary service categories, as illustrated in Figure 1 [6]:

Enhanced Mobile Broadband (eMBB), Ultra-Reliable Low-Latency Communications (URLLC), and Massive Machine-Type Communications (mMTC).

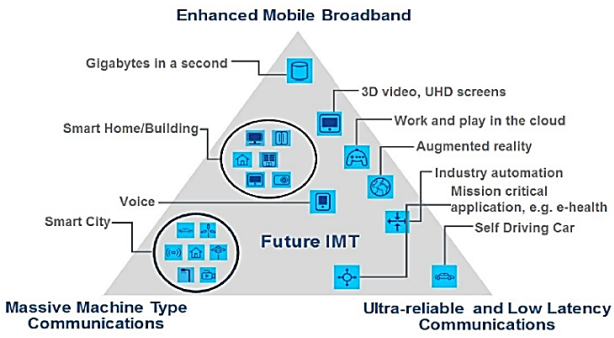

Figure 1. 5G-NR system use cases according to IMT-2020 [6].

The 3GPP Release 18 specification defines target peak data rates exceeding 10 gigabits per second (Gb/s) per cell for the Enhanced Mobile Broadband (eMBB) use case [7]. While eMBB primarily targets high data rates, it also aims to deliver a low-latency user experience, with an objective of 1 ms latency for users in motion. To achieve these ambitious targets, 5G systems leverage a suite of advanced technologies, including mmWave spectrum, small cell densification, Massive MIMO, and beamforming [8, 9].

Operating at higher frequencies than their 4G counterparts, 5G networks face inherent challenges related to signal propagation, such increased path loss and susceptibility to blockage. These challenges are mitigated through the application of sophisticated antenna technologies and advanced signal processing techniques to ensure robust and reliable network performance [10].

In the context of 5G, mmWave generally refers to the frequency range between 24 GHz and 100 GHz. This spectrum offers immense bandwidth potential, enabling exceptionally high data rates, particularly when combined with modern channel coding schemes.

5G deployments utilize a heterogeneous spectrum strategy, operating across licensed, unlicensed, and shared bands within two primary frequency ranges. Frequency Range 1 (FR1 or "sub-6 GHz") spans from 410 MHz to 7.125 GHz, encompassing low- and mid-band frequencies. Frequency Range 2 (FR2) spans from 24.25 GHz to 52.6 GHz, occupying the lower portion of the mmWave spectrum. While "mmWave" is a broader term often describing frequencies from approximately 24 GHz to 100 GHz and beyond, FR2 represents the specific, standardized 5G allocation within this range, as illustrated in Figure 2 [11].

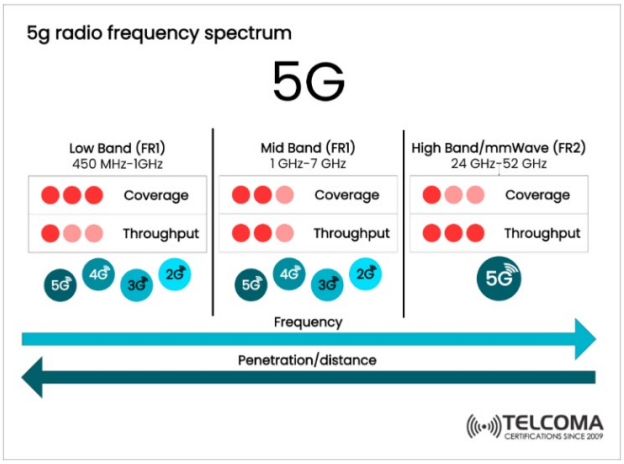

Figure 2. 5G radio frequency spectrum [11].

IV. CDL Channel Model

The Clustered Delay Line (CDL) model, standardized by the 3GPP, serves as a fundamental reference channel model for designing and evaluating 5G communication systems [12].

It is a statistical model well-suited for characterizing environments with clustered multipath propagation, where multiple signal paths arrive at the receiver in groups (clusters) with similar delay, angle, and power characteristics [13].

This makes it particularly applicable for system design in the mmWave frequency bands and for technologies like Massive MIMO. Defined for the frequency range from 0.5 GHz to 100 GHz, the CDL models are broadly categorized into two primary propagation conditions: Non-Line-of-Sight (NLOS) and Line-of-Sight (LOS). Each category is further divided into five subtypes, denoted as CDL-A, CDL-B, CDL-C, CDL-D, and CDL-E, which offer varying degrees of delay spread and K-factor to model different channel realism and severity [12, 14].

The CDL-E channel model is standardized for pure Line-of-Sight (LOS) propagation environments, representing an ideal strong direct path with minimal dependence on scattered multipath components. It is characterized by the smallest delay spread among all CDL models, reflecting very low latency variation and dominant Rician fading behavior.

This profile models a realistic LOS-dominant condition, featuring one extremely strong primary path (the direct ray) followed by very weak, short-delay multipath echoes. It is well-suited for simulating communication links in Rural Macrocell (RMa), highway, and Macrocell (UMa) scenarios, where the transmitter and receiver have a clear, unobstructed view (LOS) [12, 15]. The key parameters defining the CDL-E model are summarized in Table 1.

Table I. Parameters of the CDL-C model.[12]

Cluster #	Cluster PAS	Normalized Delay	Power in [dB]	AOD in [°]	AOA in [°]	ZOD in [°]	ZOA in [°]
1	Specular (LOS path)	0.000	-0.03	0	-180	99.6	80.4
	Laplacian	0.000	-22.03	0	-180	99.6	80.4
2	Laplacian	0.5133	-15.8	57.5	18.2	104.2	80.4
3	Laplacian	0.5440	-18.1	57.5	18.2	104.2	80.4
4	Laplacian	0.5630	-19.8	57.5	18.2	104.2	80.4
5	Laplacian	0.5440	-22.9	-20.1	101.8	99.4	80.8
6	Laplacian	0.7112	-22.4	16.2	112.9	100.8	86.3
7	Laplacian	1.9092	-18.6	9.3	-155.5	98.8	82.7
8	Laplacian	1.9293	-20.8	9.3	-155.5	98.8	82.7
9	Laplacian	1.9589	-22.6	9.3	-155.5	98.8	82.7
10	Laplacian	2.6426	-22.3	19	-143.3	100.8	82.9
11	Laplacian	3.7136	-25.6	32.7	-94.7	96.4	88
12	Laplacian	5.4524	-20.2	0.5	147	98.9	81
13	Laplacian	12.0034	-29.8	55.9	-36.2	95.6	88.6
14	Laplacian	20.6419	-29.2	57.6	-26	104.6	78.3

Per-Cluster Parameters					
Parameter	c_{ASD} in [°]	c_{ASA} in [°]	c_{ZSD} in [°]	c_{ZSA} in [°]	XPR in [dB]
Value	5	11	3	7	8

Furthermore, the CDL propagation model is fundamentally structured around discrete clusters. Each cluster comprises multiple rays that share a common propagation delay but exhibit distinct spatial characteristics, specifically through variations in their Azimuth Angle of Departure (AoD) and Azimuth Angle of Arrival (AoA) [12, 16].

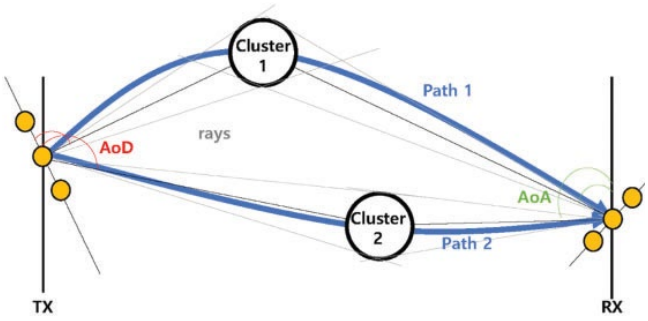

Figure 3. Concept of the CDL model [16].

V. MIMO Technology

Multiple-Input Multiple-Output (MIMO) technology enhances wireless communication by employing multiple antennas at both the transmitter and receiver. A cornerstone of modern 4G and 5G networks, MIMO enables the simultaneous transmission and reception of multiple data streams. This spatial multiplexing capability significantly increases spectral efficiency, leading to higher data throughput and improved link reliability without requiring additional bandwidth. Consequently, MIMO is a highly flexible technology for augmenting network capacity and peak data rates.

Conventional MIMO implementations typically involve a moderate number of antennas (e.g., fewer than 10) at the base station (BS) and a limited number (e.g., two or four) at the user equipment (UE), constrained by factors like physical size and hardware complexity [17, 18].

A simplified block diagram of a MIMO system is presented in Figure 4. Massive MIMO, an advanced evolution of MIMO, scales this concept by utilizing very large antenna arrays (often comprising dozens to hundreds of elements) at the base station. By leveraging this extensive spatial dimension, Massive MIMO can serve multiple users concurrently with highly focused signal beams, dramatically improving spectral efficiency, energy efficiency, and overall network capacity [18, 19].

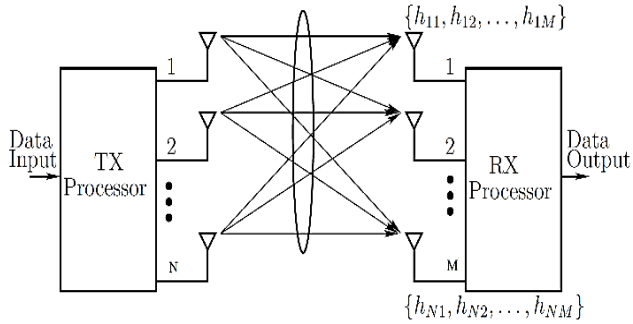

Figure 4. MIMO system block diagram. [20]

The evolution from conventional MIMO to Massive MIMO has been propelled by the escalating demand for higher data rates and the exponential growth in the number of connected devices [21].

In MIMO systems, data transmission is primarily enabled through two core techniques: spatial diversity and spatial multiplexing. Spatial diversity enhances link reliability by transmitting replicas of the same data stream across multiple independent paths. The receiver combines these signals to mitigate fading and improve the probability of correct detection.

Conversely, spatial multiplexing increases the peak data rate by splitting the data into multiple independent substreams transmitted simultaneously over different spatial channels. While this maximizes spectral efficiency, it can compromise link robustness compared to diversity schemes, creating a fundamental trade-off [23]. The general input-output relationship for a narrowband MIMO system is expressed by Equation (1) [23].

$$Y = H.X + N \ldots (1)$$

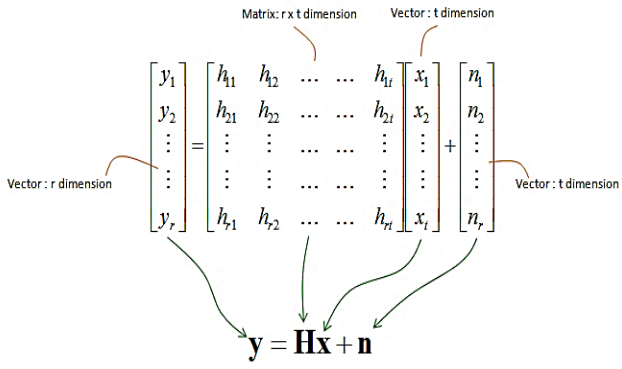

Figure 5. General MIMO equation. [20]

Where: Y is an N × 1 or (r × 1) received signal vector, H is an N × M or (r × t) channel matrix, X is an M × 1 or (t × 1) transmitted signal vector, and N represents the additive white Gaussian noise (AWGN) and it is (r × 1). This is based on the two Figures 4 and 5.

VI. Key Performance Indicators

Given the focus on the enhanced Mobile Broadband (eMBB) use case and data transmission in the mmWave frequency band, suitable key performance metrics were selected for this analysis:

1. Bit Rate:

Bit rate equation of the 5G system shown in equation (2) [24]

$$\text{Data Rate (Mbps)} = 10^{-6} \sum_{j=1}^{J} \left(v_{Layers}^{(j)} \cdot Q_m^{(j)} \cdot f^{(j)} \cdot R_{max} \cdot \frac{N_{PRB}^{BW(j),u} \cdot 12}{T_s^u} \cdot \left(1 - OH^{(j)}\right) \right) \ldots (2)$$

where J is the number of aggregated component carriers in a band or band combination; Rmax=948/1024; $v_{layers}^{(j)}$ is the maximum number of layers; $Q_m^{(j)}$ is the maximum modulation order and takes the following values (2 for QPSK, 4 for 16-QAM, 6 for 64-QAM, 8 for 256-QAM); $f^{(j)}$ is the scaling factor, the scaling factor can take the values 1, 0.8, 0.75, and 0.4. μ is the numerology (as defined in 3GPP TS 38.211) and can takes values from 0 to 5. T_S^{μ} is the average OFDM symbol duration in a subframe for numerology. $N_{PRB}^{BW(j),\mu}$ is the maximum RB allocation in bandwidth. $BW^{(j)}$ with numerology μ where $BW^{(j)}$ is the UE supported maximum bandwidth. $OH^{(j)}$ is the overhead and takes the following values: FR1 frequency range: DL: 0.14; UL: 0.08 and FR2 frequency range: DL: 0.18; UL: 0.1

2. Throughput:

Throughput can be calculated using equation (3) [22].

$$Throughput\ \left(\frac{b}{s}\right) = BW\ (Hz) \times SE\left(\frac{\frac{b}{s}}{Hz}\right) \quad (3)$$

Where BW is the bandwidth, and SE is the spectral efficiency. Or equation (2) after incorporating the effects of the Radio channel (CDL-E model here). Therefore, enhancing the achievable data rate necessitates an increase in either the channel bandwidth or the spectral efficiency. Given that the radio spectrum is a finite and often congested resource, significant bandwidth expansion is seldom feasible. Consequently, the primary focus for performance improvement shifts to maximizing spectral efficiency.

A canonical method for achieving this is the deployment of Multiple-Input Multiple-Output (MIMO) systems, which utilize multiple antennas at both link ends. MIMO technology enhances spectral efficiency by exploiting spatial diversity and multiplexing, thereby enabling high-speed data transmission even under challenging channel conditions [22].

3. Spectral efficiency:

The spectral efficiency relationship is given by equation (4) [24,25].

$$SE_{5G}\left(\frac{bps}{Hz}\right) = \frac{5G\ Throughput\ or\ R\ (bps)}{Channel\ BW(Hz)} \quad \ldots \quad (4)$$

Where, R represents the bit rate, and BW represents the bandwidth. It should be noted that bandwidth represents the maximum bandwidth supported by the User Equipment (UE) in a given frequency band or multiple bands. The Resource Elements (REs) are grouped into Physical Resource Blocks (PRBs), where each PRB consists of 12 subcarriers with a specific Subcarrier Spacing (SCS). Therefore, the actual bandwidth—excluding guard bands—can be calculated according to the new 5G radio standard using equation (5) [26].

$$BW(MHz) = NPRB \times SCS \times 12 \times 10^{-3} \quad \ldots \quad (5)$$

VII. Improving Network Throughput

Enhancing throughput in wireless communication systems presents a significant engineering challenge. The network throughput, often defined as the total data rate successfully delivered over a given coverage area, can be modeled by the general expression in Equation (6) [27].

$$Area\ throughput\left(\frac{\frac{b}{s}}{km^2}\right) = BW(Hz) \times CD\left(\frac{cells}{km^2}\right) \times SE\left(\frac{\frac{b}{s}/Hz}{Cell}\right) \quad \ldots \quad (6)$$

where BW is the allocated channel bandwidth, CD represents the network cell density (e.g., base stations per km²), and SE is the average spectral efficiency (in bits/s/Hz). A fundamental physical-layer challenge is to reliably and

uniformly enhance the aggregate wireless throughput across a target coverage area [27]. As indicated by Equation (5) and established in prior studies [28, 29], achieving higher throughput relies on three principal levers:

1) **Bandwidth Expansion:** Allocating additional spectrum to 5G services.
2) **Network Densification:** Condensing the network topology by deploying more cells and access points.
3) **Spectral Efficiency Enhancement:** Utilizing technologies like Multiple-Input Multiple-Output (MIMO) to improve the data transmission efficiency per cell within a fixed bandwidth.

Accordingly, the objective of this research is to evaluate the end-to-end performance of 5G mmWave communication systems under varied scenarios and parameter configurations. The analysis is based on three key performance metrics—spectral efficiency, transmitted bit rate, and achievable throughput—for a given channel bandwidth.

VIII. Implementation and Results

This paper investigates the application of multi-layer transmission (spatial multiplexing) in 5G mmWave communication systems operating at 40 GHz, corresponding to the 3GPP FR2 band n260. The primary objective is to demonstrate a significant enhancement in system performance—specifically in data transmission quality—by improving key performance indicators (KPIs) for the enhanced Mobile Broadband (eMBB) use case, such as spectral efficiency and throughput, under realistic Line-of-Sight (LOS) propagation conditions modeled using the 3GPP CDL-E channel model.

The proposed approach targets performance gains at both the transmitter, through layered data streams, and the receiver, leveraging Multiple-Input Multiple-Output (MIMO) signal processing with practically realizable antenna configurations for user equipment. The analysis focuses on the downlink (DL) transmission scenario.

The primary contribution of this work is twofold. First, it demonstrates the efficacy of the multi-layer transmission (spatial multiplexing) concept in significantly improving the achievable bit rate at the transmitter (Tx). We quantify this performance gain and analyze its scalability with an increasing number of layers.

Second, the study reveals a critical limitation: these transmitter-side gains do not directly translate to proportional improvements at the receiver (Rx) without additional signal processing support. To address this, we employ Multiple-Input Multiple-Output (MIMO) precoding techniques using Singular Value Decomposition (SVD) to recover the spatial streams and mitigate inter-layer interference. The use of multiple codewords, as defined in 3GPP specifications, provides greater flexibility in controlling the Modulation and Coding Scheme (MCS) for each codeword independently.

The system was implemented, and simulated using MATLAB R2024a. Figure 6 illustrates the block diagram of the implemented 5G NR downlink transmission system.

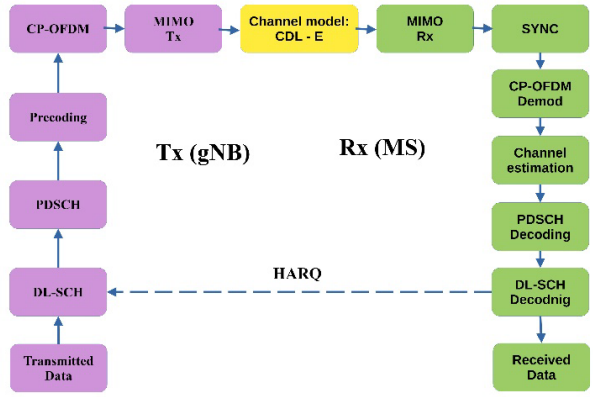

Figure 6. The block diagram of the implemented system.

The architecture supports multi-layer spatial multiplexing with independent control over the number of transmission layers and the antenna array dimensions at both the transmitter (gNB) and receiver (UE). The system employs Singular Value Decomposition (SVD)-based precoding at the transmitter to separate the spatial streams, which effectively performs digital beamforming, and MIMO processing at the receiver to recover the transmitted data. A key feature is the use of multiple codewords, each associated with an independent Modulation and Coding Scheme (MCS), providing flexible link adaptation.

The Demodulation Reference Signal (DMRS) symbols are allocated within each time slot according to 3GPP specifications. which according to the 3GPP TS 138 211 specification, the following conditions must be satisfied: the number of transmit and receive antennas must be at least equal to the number of spatial layers $(N_{TX}, N_{RX}) \geq N_{\text{layers}}$, and the DMRS length is configured as a function of the layer count: DMRS length = 1 for $N_{\text{layers}} \leq 4$, and DMRS length = 2 for $4 < N_{\text{layers}} \leq 8$.

In the results section, we present the effect of varying the number of layers and the number of antennas on the data transmission performance of the system. The primary simulation parameters are listed in Table II. For the scope of this analysis, we apply a uniform MCS across all layer.

Table II. Simulation parameters

Parameter	Value
Number of frames	1
SNR (dB)	-2 to 8
PRBs	135
SCS (kHz)	60
CP	Normal
Mapping Type	A
1st Modulation Order	16QAM
1st Code Rate	0.5
2nd Modulation Order	16QAM
2nd Code Rate	0.5
MIMO (Tx)	16, 32
MIMO (Rx)	4, 8
Channel model (Delay Profile)	CDL-E
Delay Spread (μsec)	300
Frequency (GHz)	40
Num of HARQ Processes	16
Waveform Type	CP-OFDM
Channel BW (MHz)	100

Three distinct MIMO system configurations, denoted by their antenna dimensions $N_t \times N_r$, are evaluated in this study. These scenarios are designed to isolate the impact of spatial multiplexing and antenna scaling. The configurations are as follows:

Scenario 1 (Baseline): A single codeword is transmitted using a 16 × 4 MIMO configuration. The number of spatial layers is varied from 1 to 4, corresponding to the maximum rank supported by this antenna configuration.

Scenario 2 (Multi-Layer with Fixed Antennas): Two independent codewords are transmitted concurrently using the same 16 × 8 MIMO configuration as Scenario 1. The number of spatial layers is varied from 5 to 8.

Scenario 3 (Multi-Layer with Antenna Scaling): Two independent codewords are transmitted using an expanded MIMO configuration of 32 × 8 antennas. The number of spatial layers is again varied from 5 to 8.

This progression allows for a comparative analysis of performance gains attributable to spatial multiplexing (Scenario 2) versus the combined effect of multiplexing and increased spatial degrees of freedom (Scenario 3).

The choice of 4 and 8 receive antennas at the UE reflects practical hardware constraints in commercial mobile devices, where physical size, power consumption, and thermal limitations restrict the number of antenna elements that can be integrated. These configurations are sufficient to support up to 4 spatial layers for the single-codeword scenario and up to 8 spatial layers for the dual-codeword scenario, respectively, which represent the maximum numbers considered in this study.

Case 1: 16 × 4 MIMO with a Single Codeword

The throughput and spectral efficiency (SE) performance for a 16 × 4 MIMO configuration employing a single codeword (mapped to 1 to 4 spatial layers) are presented in Figures 7, 8, and 9, respectively.

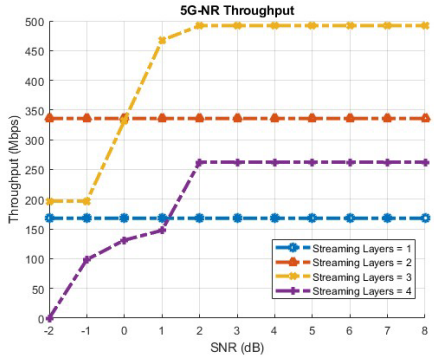

Figure 7. Throughput of the 5G-NR system using a single codeword with 16 × 4 MIMO.

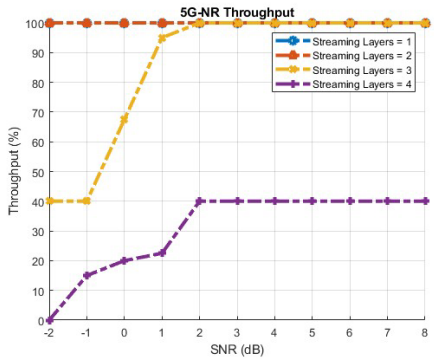

Figure 8. Normalized throughput (% of peak theoretical rate) of the 5G-NR system using a single codeword with 16 × 4 MIMO.

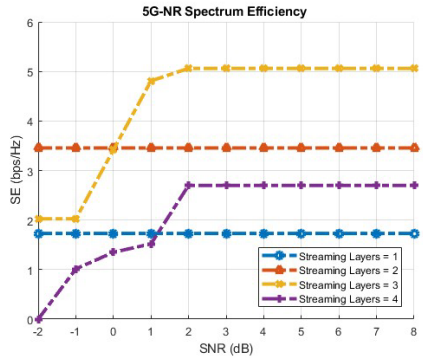

Figure 9. Spectral efficiency of the 5G-NR system using a single codeword with 16 × 4 MIMO.

Case 2: 16 × 8 MIMO with Dual Codewords

The corresponding throughput and spectral efficiency (SE) results for a 16 × 8 MIMO system utilizing two independent

codewords (mapped to 5 to 8 spatial layers) are presented in Figures 10, 11, and 12, respectively.

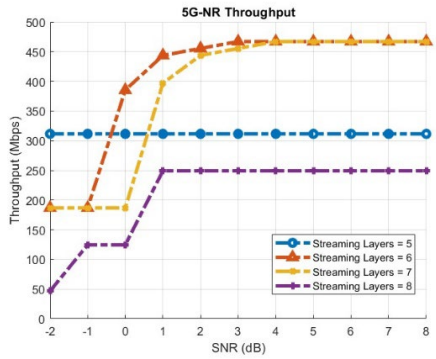

Figure 10. Throughput of the 5G-NR system using dual codewords with 16 × 8 MIMO.

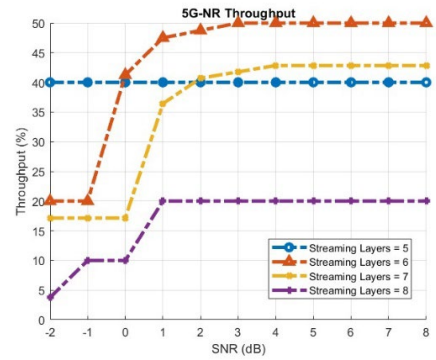

Figure 11. Normalized throughput (% of peak theoretical rate) of the 5G-NR system using dual codewords with 16 × 8 MIMO.

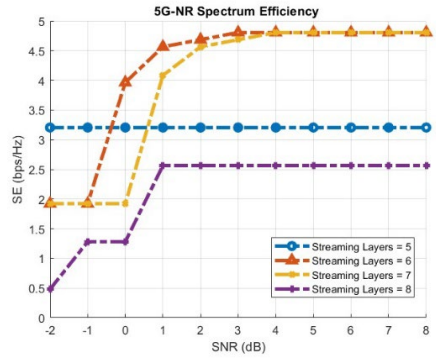

Figure 12. Spectral efficiency of the 5G-NR system using dual codewords with 16 × 8 MIMO.

The increase to 8 receive antennas is necessary to support up to 8 spatial layers, as the condition $N_{Rx} \geq N_{layers}$ must be satisfied. While this represents an optimistic upper bound for current UE hardware, it allows us to evaluate the maximum potential of spatial multiplexing in the dual-codeword scenario.

Case 3: 32 × 8 MIMO with Dual Codewords

Figures 13, 14, and 15 present the throughput and spectral efficiency (SE) for an expanded 32 × 8 MIMO configuration, maintaining the use of two independent codewords (mapped to 5 to 8 spatial layers).

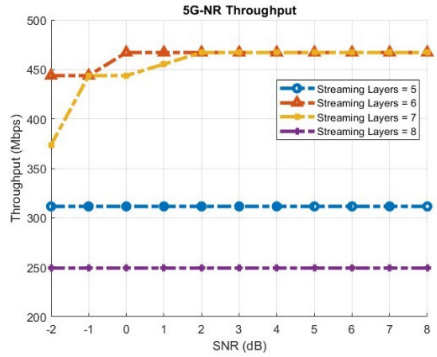

Figure 13. Throughput of the 5G-NR system using dual codewords with 32 × 8 MIMO.

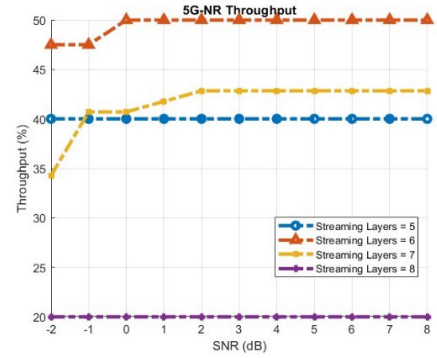

Figure 14. Normalized throughput (% of peak theoretical rate) of the 5G-NR system using dual codewords with 32 × 8 MIMO.

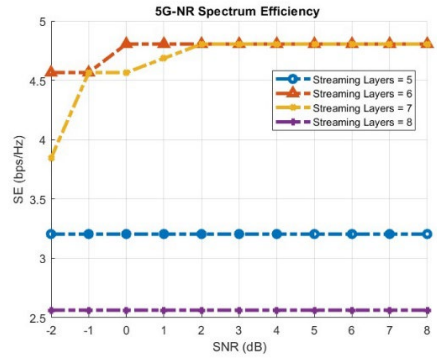

Figure 15. Spectral efficiency of the 5G-NR system using dual codewords with 32 × 8 MIMO.

Finally, Figures 16, 17, and 18 illustrate the variation of three key metrics—peak throughput, peak spectral efficiency, and user-experienced data rate (as a percentage of the maximum)—as a function of the number of spatial (streaming) layers.

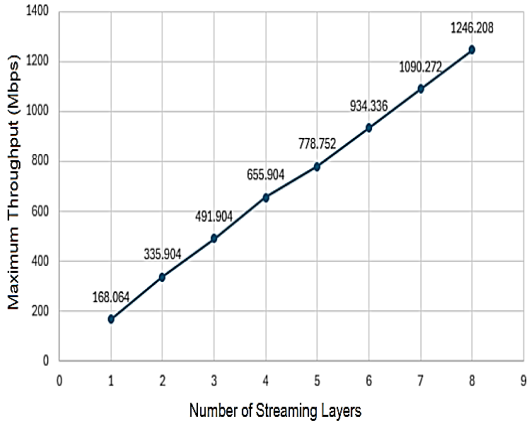

Figure 16. Bit Rate versus the number of spatial layers.

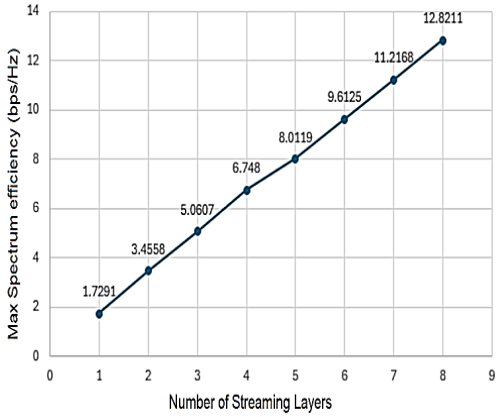

Figure 17. Maximum spectral efficiency versus the number of spatial layers.

IV. Discussion

This section provides a comprehensive analysis of the simulation results presented in Figures 7–15. The discussion is structured according to the three investigated scenarios, each defined by a specific MIMO configuration and range of spatial layers. All simulations were conducted at 40 GHz using the 3GPP CDL-E channel model, which represents a realistic Line-of-Sight (LOS) propagation environment with rich angular dispersion.

Scenario A (Tx = 16, Rx = 4, Layers 1–4), Figures 7, 8, and 9 illustrate the normalized throughput (%), absolute throughput (Mbps), and spectral efficiency (bps/Hz) for a single codeword transmitted over 1 to 4 spatial layers.

Low SNR regime (SNR < 0 dB): At very low Signal-to-Noise Ratio (SNR), thermal noise dominates the link. Consequently, configurations with fewer layers (e.g., 1 or 2 layers) achieve higher normalized throughput than those with 3 or 4 layers. This is because the channel lacks sufficient capacity to support reliable demultiplexing of multiple spatial streams under noisy conditions.

High SNR regime (SNR ≥ 2 dB): As SNR increases, the advantage of spatial multiplexing becomes evident. For example, at SNR = 2 dB, the 3-layer configuration reaches 100% normalized throughput, while the 4-layer configuration reaches 40%. In absolute terms, the 4-layer setup delivers ~260 Mbps compared to only ~170 Mbps for a single layer. This demonstrates that increasing the number of spatial layers significantly enhances spectral efficiency when channel conditions are favorable.

Practical insight: With 4 receive antennas at the User Equipment (UE), supporting up to 4 layers represents a realistic upper bound for commercial devices. The results confirm that this configuration can fully exploit the available spatial degrees of freedom at moderate to high SNR.

Scenario B (Tx = 16, Rx = 8, Layers 5–8), Figures 11, 12, and 13 show the performance when transmitting two independent codewords mapped to 5 to 8 spatial layers, while keeping the number of transmit antennas at 16 and increasing receive antennas to 8.

Limited effective rank: Despite increasing the number of receive antennas to 8, the system struggles to support more than 4 effective layers. At SNR = 8 dB, the normalized throughput for 5 layers is only 40%, dropping to 20% for 8 layers. This indicates that with only 16 transmit antennas and the CDL-E channel model, the effective rank of the channel matrix is limited to approximately 2.

Non-linear behavior (Layers 6 and 7 outperforming Layer 5): A notable observation in Figures 11 and 12 is that at moderate SNR values (e.g., 0–4 dB), the throughput for 6 and 7 layers exceeds that of 5 layers. This counterintuitive behavior arises from the Transport Block Size (TBS) quantization and Code Block Segmentation procedures defined in 3GPP NR. Specifically:

Layer 5 falls into an unfavorable quantization region, leading to a lower effective code rate and higher overhead.

Layers 6 and 7 achieve better alignment with the code block size limits, resulting in larger TBS and more efficient utilization of the available resources.

This finding underscores that performance is not a simple linear function of the number of layers; rather, it is influenced by higher-layer procedural effects.

Inter-layer interference: As the number of layers increases beyond the effective rank, inter-layer interference (ILI) becomes severe. The receiver, even with 8 antennas, cannot fully suppress this interference, leading to degraded throughput despite the higher theoretical peak rate.

Scenario C (Tx = 32, Rx = 8, Layers 5–8), Figures 13, 14, and 15 present the results for an expanded configuration with 32 transmit antennas at the gNB while maintaining 8 receive antennas at the UE. This scenario isolates the impact of increasing spatial degrees of freedom at the transmitter.

Improved array gain: Compared to Scenario B, the 32-transmit configuration exhibits a clear shift of the throughput curves toward lower SNR. For example, at SNR = 0 dB, the normalized throughput for 8 layers increases from 10% (Scenario B) to 20% (Scenario C). This improvement is attributed to the higher array gain provided by the larger antenna array, which enhances the received signal power without increasing transmit power.

Enhanced support for higher layers: Increasing the number of transmit antennas to 32 raises the statistical probability of a higher channel rank. At SNR = -2 dB, the normalized throughput for 8 layers reaches 20% in Scenario C, compared to only 4% in Scenario B. This demonstrates that massive MIMO at the base station is a key enabler for high-order spatial multiplexing in mmWave bands.

Remaining bottleneck: Even with 32 transmit antennas, the performance for 8 layers saturates at 20% (not 100%). This limitation is due to the receive antenna count (8) , which now becomes the limiting factor. With only 8 receive antennas, the system cannot fully resolve 8 independent spatial streams under realistic CDL-E channel conditions, which impose spatial correlation.

The comparison clearly shows that scaling the number of transmit antennas at the gNB significantly improves both the achievable throughput and the robustness against inter-layer interference, even when the number of receive antennas remains constant.

Figures 16 and 17 illustrate the peak theoretical bit rate and maximum spectral efficiency as functions of the number of spatial layers, respectively. Both metrics exhibit an approximately linear relationship with the number of layers, as expected from the fundamental MIMO capacity formula. For instance, increasing the number of layers from 1 to 8 raises the peak bit rate from 168 Mbps to 1246 Mbps, and the spectral efficiency from 1.73 bps/Hz to 12.82 bps/Hz.

However, these values represent an upper-bound benchmark achievable only under ideal channel conditions with no noise, no interference, and perfect receiver processing. In practice, as demonstrated in Figures A1–C3, the actual user throughput is significantly lower, particularly for higher layer counts and lower SNR values.

The gap between the peak theoretical rate and the achieved throughput highlights the impact of inter-layer interference, channel rank limitations under the CDL-E model, and the finite capabilities of the MIMO receiver.

The non-uniform incremental gains observed between successive layer counts (e.g., the marginal increase from 4 to 5 layers is 131 Mbps, while from 7 to 8 layers it is 219 Mbps) are attributed to the Transport Block Size (TBS) quantization and code block segmentation procedures inherent to the 3GPP NR standard.

These procedural effects introduce rounding and alignment constraints that cause the peak rate to deviate slightly from perfect linearity. Overall, Figures 16 and 17 confirm that spatial multiplexing is a powerful enabler for high-data-rate transmission in 5G mmWave systems, while also underscoring the need for advanced receiver processing and sufficient antenna resources to approach the theoretical limits in practical deployments.

X. Conclusion and Future Work

This paper investigated the performance of multi-layer spatial multiplexing in a 5G NR downlink system operating at 40 GHz (3GPP FR2 band n260) using the CDL-E channel model for realistic Line-of-Sight propagation. The study focused on the impact of the number of spatial layers and MIMO antenna configurations on key performance indicators, namely throughput and spectral efficiency, under practically feasible UE antenna constraints (4 and 8 receive antennas).

The experimental findings yield the following scientific insights: Non-linear relationship between layers and throughput: Increasing the number of spatial layers does not guarantee a proportional increase in user throughput.

Performance is governed by the effective channel rank, the TBS quantization effects inherent to 3GPP NR, and the balance between transmit and receive antennas. This was particularly evident in Scenario B, where layers 6 and 7 outperformed layer 5 due to more favorable code block segmentation.

Massive MIMO at the gNB is essential for mmWave: The transition from 16 to 32 transmit antennas (Scenario C) resulted in a substantial improvement in both array gain and spatial multiplexing capability. At SNR = -2 dB, the normalized throughput for 8 layers increased from 4% to 20%, confirming that massive MIMO at the base station is a critical enabler for high-order spatial multiplexing in the FR2 band.

UE antenna count remains a practical bottleneck: While increasing transmit antennas improves performance, the receive antenna count at the UE (4 or 8) ultimately limits the maximum achievable rank. Even with 32 transmit antennas, the 8-layer configuration could not reach 100% normalized throughput, indicating that further gains require more advanced UE antenna designs or collaborative MIMO schemes. Trade-off between layers and SNR: Systems with fewer spatial layers (e.g., 1–4 layers) achieve near-100% throughput efficiency at lower SNR values and require fewer receive antennas.

This makes them suitable for cell-edge users or devices with tight form-factor constraints. Conversely, higher-order multiplexing (5–8 layers) delivers superior peak throughput but demands higher SNR and more sophisticated interference

mitigation. Flexibility through multi-codeword transmission: The use of multiple independent codewords, each with its own Modulation and Coding Scheme (MCS), provides valuable adaptability.

This allows the system to optimize link performance based on real-time channel conditions, user requirements, and quality-of-service (QoS) targets. In summary, this work demonstrates that practical, commercially relevant UE antenna configurations (4–8 Rx) can support up to 8 spatial layers when combined with massive MIMO at the gNB (32 Tx) , provided that the channel conditions (LOS, CDL-E) are favorable.

The results also highlight the importance of considering higher-layer procedural effects (TBS quantization, code block segmentation) when evaluating MIMO performance, as these can lead to non-intuitive behaviors such as higher layers outperforming lower ones.

Future research directions include:

- Investigating hybrid beamforming architectures that better reflect practical mmWave implementations.
- Exploring higher receive antenna counts (e.g., 16 or 32) at the UE, possibly through collaborative or distributed MIMO approaches.
- Analyzing the impact of imperfect channel estimation and realistic HARQ processes on multi-layer performance.
- Extending the analysis to multi-user MIMO (MU-MIMO) scenarios with inter-user interference.

REFERENCES

[1] Ashraf, A., Gunawan, T. S., Kartiwi, M., Nur, L. O., Nugroho, B. S., & Astuti, R. P. (2024). Advancements and challenges in scalable modular antenna arrays for 5G massive MIMO networks. *IEEE Access*, 12, 57 895–57 916.

[2] Nkrumah, M. (2023). The Impact of 5G Technology on Communication Infrastructure. *Journal of Communication*, 4(1), 43–55. DOI: 10.47941/jcomm.1655

[3] Alrubaye, J. S., Abdkhaleq, M. H. G., & Alaidi, A. H. (2024). A Comprehensive Review of Routing in 4G/5G Cellular Networks: Challenges, Trends, and Future Directions. *Journal of Al-Qadisiyah for Computer Science and Mathematics*, 16(4), 215–230. DOI: 10.29304/jqcsm.2024.16.41784

[4] Ashraf, S., Sheikh, J. A., Ashraf, A., & Rasool, U. (2024). 5G Millimeter Wave Technology: An Overview. In book: *Intelligent Signal Processing and RF Energy Harvesting for State of Art 5G and B5G Networks*. Springer, 97–112. DOI: 10.1007/978-981-99-8771-9_6

[5] Földes, G. (2023). Techno-Economic Analysis on Mobile Network Sharing Contribution to Social Welfare at 4G–5G Area in Hungary. *Infocommunications Journal*, 15(1), 87–97, DOI: 10.36244/icj.2023.1.9

[6] Shafi, M., et al., (2017). 5G: A Tutorial Overview of Standards, Trials, Challenges, Deployment, and Practice. *IEEE Journal on Selected Areas in Communications*, 35(6), 1201–1221. DOI: 10.1109/jsac.2017.2692307

[7] Makara, Á. L., & Csurgai-Horváth, L. (2021). Improved Model for Indoor Propagation Loss in the 5G FR2 Frequency Band. *Infocommunications Journa*l, 13(1), 2–10. DOI: 10.36244/icj.2021.1.1

[8] Zreikat, A. I., & Mathew, S. (2024). Performance evaluation and analysis of urban-suburban 5g cellular networks. *Computers*, 13(4), 108.

[9] Marinova, S., & Leon-Garcia, A. (2024). Intelligent O-RAN Beyond 5G: Architecture, Use cases, Challenges, and Opportunities. *IEEE Access*, 12, 27 088–27 114 DOI: 10.1109/access.2024.3367289.

[10] Islam, S., Abdulsalam, A. Z., Kumar, B. A., Hasan, M. K., Kolandaisamy, R., & Safie, N. (2024). Mobile Networks Toward 5G/6G: Network Architecture, Opportunities and Challenges in Smart City. *IEEE Open Journal of the Communications Society,* 6, 3082–3093. DOI: 10.1109/ojcoms.2024.3419791

[11] https://telcomaglobal.com/p/5g-frequency-bands

[12] ETSI. "TS 138 901 V17.0.0 (2022-04) – 5G; Study on channel model for frequencies from 0.5 to 100 GHz (3GPP TR 38.901 Release 17).

[13] Zhu, Q. et al. (2019). 3GPP TR 38.901 Channel Model. Chapter in Wiley 5G Ref: The Essential 5G Reference Online. *John Wiley & Sons*. DOI: 10.1002/9781119471509.w5gref048

[14] Zhang, Y., Sun, J., Gui, G., Gacanin, H., & Adachi, F. (2022). A Novel Channel Identification Architecture for mmWave Systems Based on Eigen Features. *IEEE 14th International Conference on Wireless Communications and Signal Processing (WCSP)*, 550–555. DOI: 10.1109/wcsp55476.2022.10039221

[15] Kumari, N., Rajput, R., & Sharma, S. (2023). CDL Channel Model: Revolutionizing Wireless Communication. *International Journal of Innovative Science and Research Technology,* 8(7), 1937–1949.

[16] Lee, K.H. (2022). LCF: A Deep Learning-Based Lightweight CSI Feedback Scheme for MIMO Networks. *Computers, Materials & Continua*, 71(3), 5561–5580. DOI: 10.32604/cmc.2022.024562

[17] Bhatti, U.S. (2025). Performance Enhancement of 5G Networks Remodeling Power Domain Scheme through NOMA-MIMO Technologies Integration. *International Journal of Advanced Engineering, Management and Science,* 11(4), 280–300. DOI: 10.22161/ijaems.114.28

[18] De Figueiredo, F. A. P. (2022). An overview of massive MIMO for 5G and 6G. *IEEE Latin America Transactions*, 20(6), 931–940.

[19] Jwair, M. H., & Elwi, T. A. (2023). Meta Surface Antenna Circuitry for 5G Communication Networks. *Infocommunications Journal,* 15(2), 2–7. DOI: 10.36244/icj.2023.2.1

[20] Halak, B., *et al*. (2018). Hardware Efficient Architecture for Element-Based Lattice Reduction Aided K-Best Detector for MIMO Systems. *Journal of Sensor and Actuator Networks*, 7(22), 1–16. DOI: 10.3390/jsan7020022

[21] Lu, L., Li, G. Y., Swindlehurst, A. L., Ashikhmin, A., & Zhang, R. (2014). An Overview of Massive MIMO: Benefits and Challenges. *IEEE Journal of Selected Topics in Signal Processing*, 8(5), 742–758. DOI: 10.1109/jstsp.2014.2317671

[22] Borges, D., Montezuma, P., Dinis, R., & Beko, M. (2021). Massive mimo techniques for 5g and beyond—opportunities and challenges. *Electronics*, 10(14), 1667.

[23] Baghous, J. (2021). 5G System Throughput Performance Evaluation using Massive-MIMO Technology with Cluster Delay Line Channel Model and Non-Line of Sight Scenarios. *Infocommunications Journal*, 13(2), 40–45. DOI: 10.36244/icj.2021.2.6

[24] 3GPP TS 38.306 v15.7.0, (2019-09). 5G-NR-User Equipment (UE) Radio Access Capabilities. (Release 15).

[25] Barri, E., Bouras, C., Kokkinos, V., & Koukouvela, A. (2021, November). A Mechanism for Improving the Spectral Efficiency in mu-MIMO for 5G and Beyond Networks. In *Proceedings of the 19th ACM International Symposium on Mobility Management and Wireless Access* (pp. 11–16).

[26] Furht, B. (2012). Encyclopedia of Wireless and Mobile Communications. *CRC Press*. DOI: 10.1201/noe1420043266

[27] 3GPP TS 38.101-1 version 15.3.0, (2018-10). 5G-NR-User Equipment (UE) Radio Transmission and Reception; Part 3: Range 1 and Range 2. (Release 15).

[28] Marzetta, T. L. (2015). Massive MIMO: an Introduction. *Bell Labs Technical Journal*, 20, 11–22. DOI: 10.15325/bltj.2015.2407793

[29] Xiang, W., Zheng, K., and Shen, X. (Eds). (2017). *5G Mobile Communications*. Springer. DOI: 10.1007/978-3-319-34208-5

John Baghous received his BE in Electronics and Communications Engineering (2017) from Damascus University (DU), Syria, and his Master in Advanced Communications Engineering (2021) from DU. His is currently a PhD student at the department of Electronics and Communications Engineering, Faculty of Mechanical and Electrical Engineering, DU, Syria. His research areas include cellular communications, wireless communication, wireless sensor networks, and D2D communications.

Mohamed Khaled Chahine received his BE in Electronics (1985) from INPG Grenoble France, Postgraduate MEng in Electronics and Optoelectronics (1990), and PhD in Satellite Communications (1994) from University of Pierre and Marie Curie Paris France. From 1994 to 2004, he was working at HIAST Damascus Syria as researcher and teacher. From 2004 to 2006 he was Director of COMSAT-COMSTECH-ITC Syria. Since 2006, he is an Associate Professor at the Department of Electronics and Communication Engineering at the Faculty of Mechanical and Electrical Engineering at Damascus University, Syria. His research areas include satellite communications, mobile communications, communication networks, optical communications, electronics engineering, wireless sensor networks, vehicular communications, software-defined networks, software-defined radios, quality control, ground penetrating radar, and audio and video streaming.